

Electronic Supplementary Information

**Boosting Energy Storage Performance with Lead-Free Relaxor Ferroelectric in
BNT-Based Ceramics via Introducing Scheelite La_2WTiO_8**

Wenyuan Li ^{a,b}, Jianan Xu ^{a,b}, Jia Chen ^{a,b}, Yaxin Wei ^a, Kai Li ^c, Aimin Chang ^a, Bo Zhang ^{a,*}

^a*State Key Laboratory of Functional Materials and Devices for Special Environmental Conditions; Xinjiang Key Laboratory of Electronic Information Materials and Devices; Xinjiang Technical Institute of Physics & Chemistry of CAS, Urumqi, 830011, China*

^b*Center of Materials Science and Optoelectronics Engineering, University of Chinese Academy of Sciences, Beijing, 100049, China*

^c*Changchun Institute of Applied Chemistry of CAS, Changchun 130022, China*

* Corresponding author

E-mail addresses: zhangbocas@ms.xjb.ac.cn (B. Zhang)

1. DFT computational method

In the Density-functional theory (DFT) calculations of the BNLTW-0.09 properties, the generalized gradient approximation (GGA) in the flavor of the Perdew-Burke-Ernzerhoff (PBE) functional was utilized to handle the exchange-correlation interactions. The valence electron configurations were $6s^24f^{14}5d^{10}6p^3$, $3s^1$, $4s^23d^2$, $6s^25d^1$, $6s^24f^{14}5d^4$ and $2s^22p^4$ for Bi, Na, Ti, La, W and O atoms, respectively. The Broyden-Fletcher-Goldfarb-Sanno (BFGS) algorithm was used to carry out the geometric optimization, which continued until the maximum force dropped to a value below 0.01 eV/Å, ensuring that the system reached a stable equilibrium and that the energies converged to a level below 1×10^{-6} eV/atom, demonstrating a high degree of accuracy in the calculations. The self-consistent field tolerance was set to 1×10^{-6} eV/atom, a parameter that determined the convergence criterion for electronic structure calculations. The maximum number of cycles allowed for the self-consistent field iteration was set to 200, ensuring that the calculation did not run indefinitely. Additionally, a k -point grid of $8\times4\times8$ was utilized for the Brillouin zone sampling, which is important for accurate calculations of electronic properties in periodic systems.

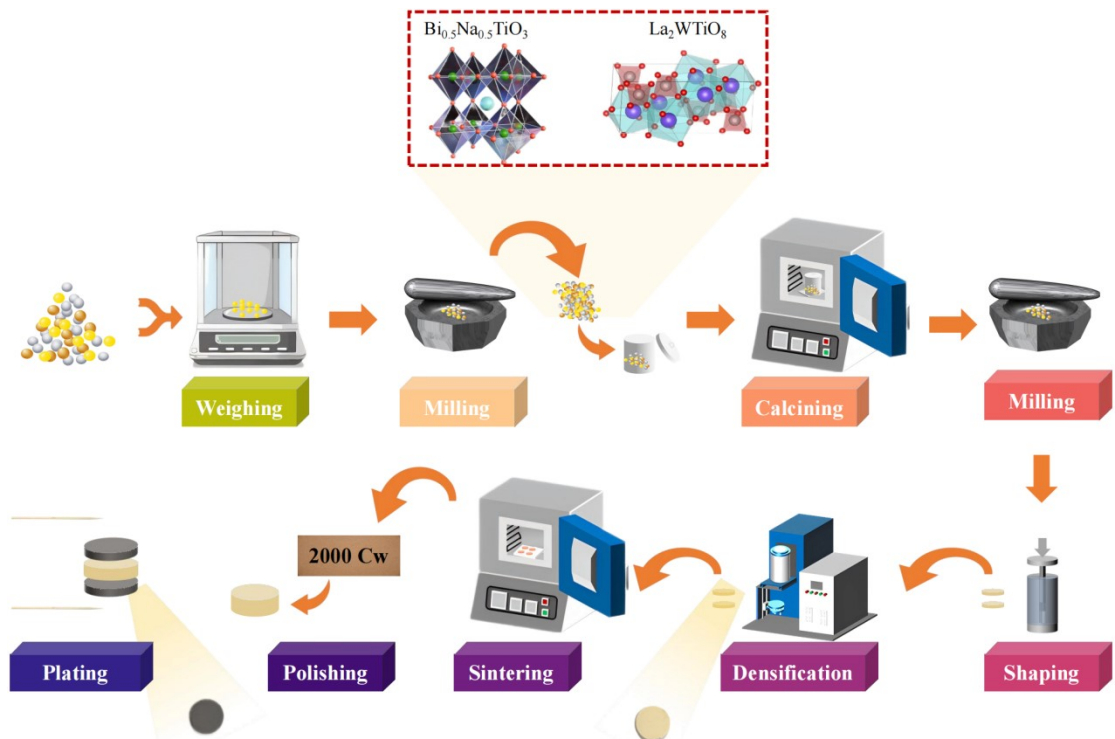


Figure S1. Schematic diagram of the synthesis process.

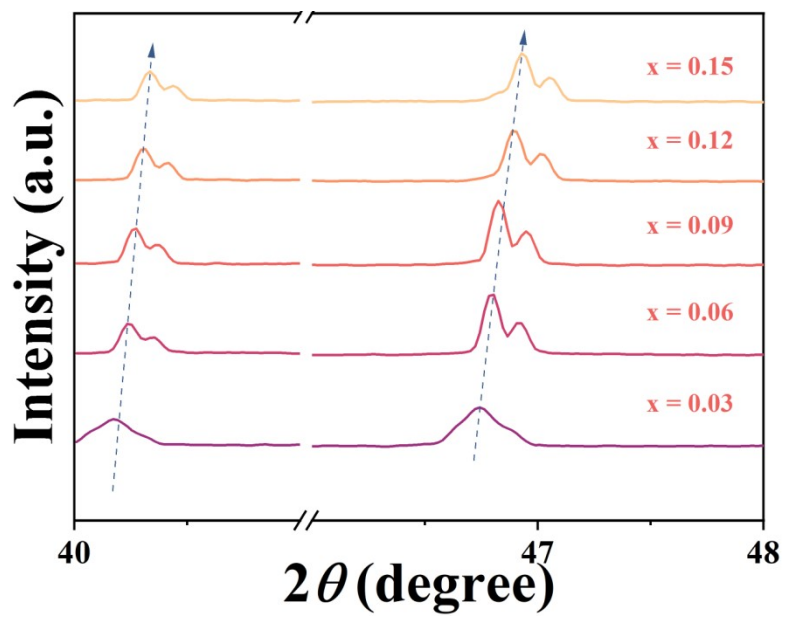


Figure S2. XRD patterns of the enlarged patterns of $38\text{-}48^\circ$.

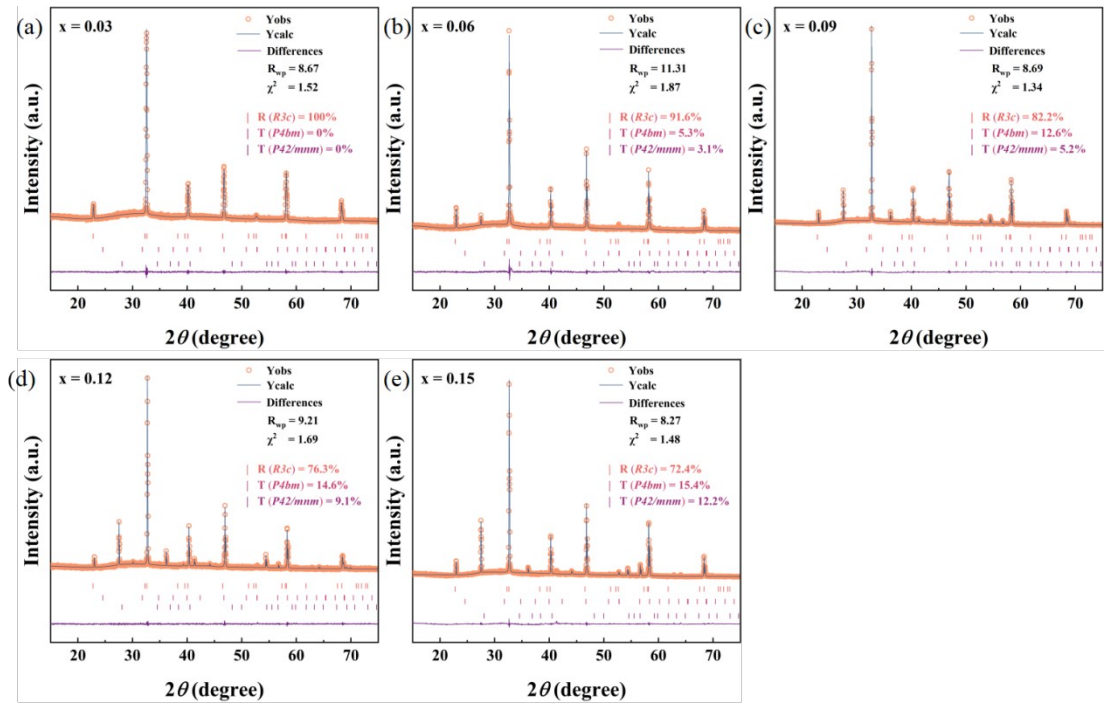


Figure S3. Rietveld refinement analysis of BNLTW- x ceramics.

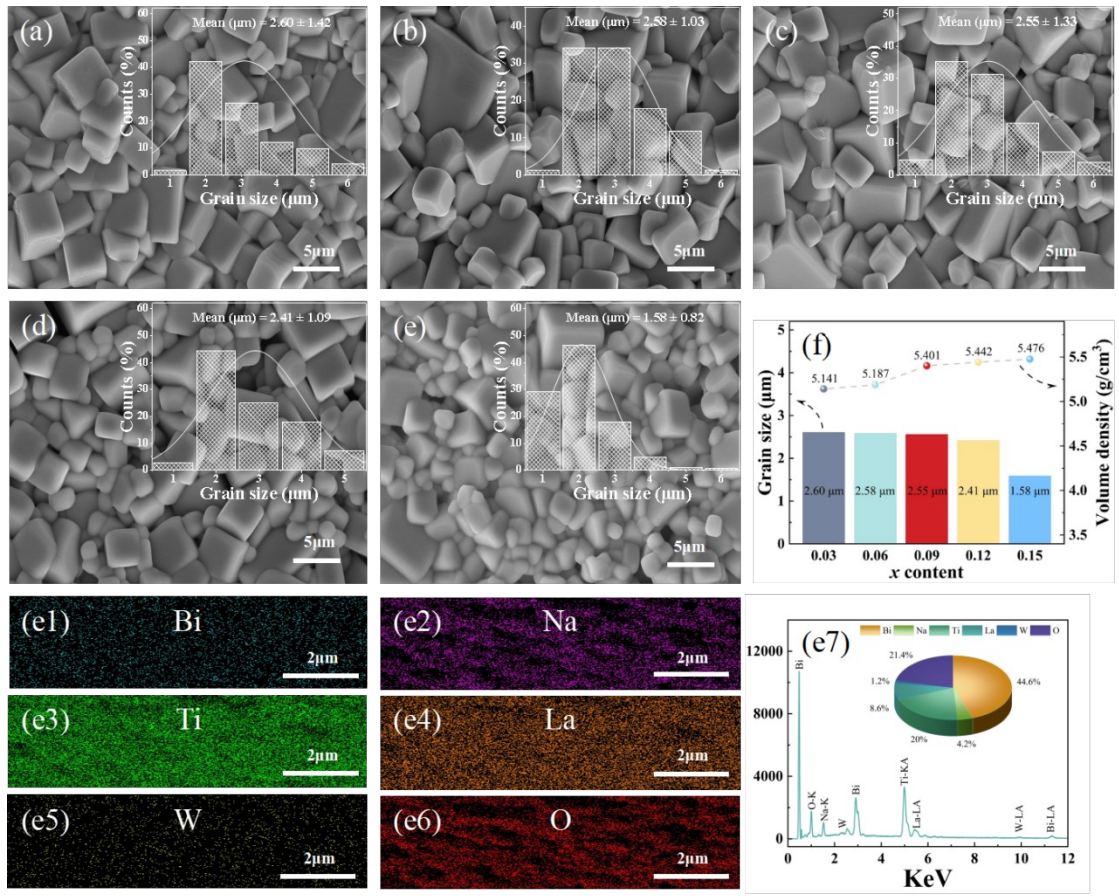


Figure S4. SEM images of BNLTW- x ceramics, (a) $x = 0.03$, (b) $x = 0.06$, (c) $x = 0.09$, (d) $x = 0.12$, (e) $x = 0.15$; (f) Evolution of grain size and volume density as a function of x ; (e1-e6) Backscattered electron image and chemical-element mappings of the sample ($x = 0.15$) and (e7) EDS spectra.

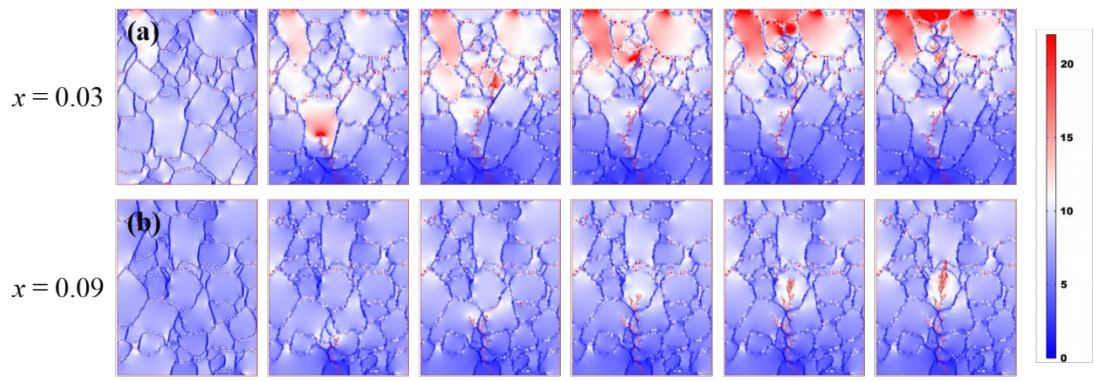


Figure S5. Polarisation distribution of (a) BNLTW-0.03 ceramic and (b) BNLTW-0.09 ceramic at 300 kV cm^{-1} voltage.

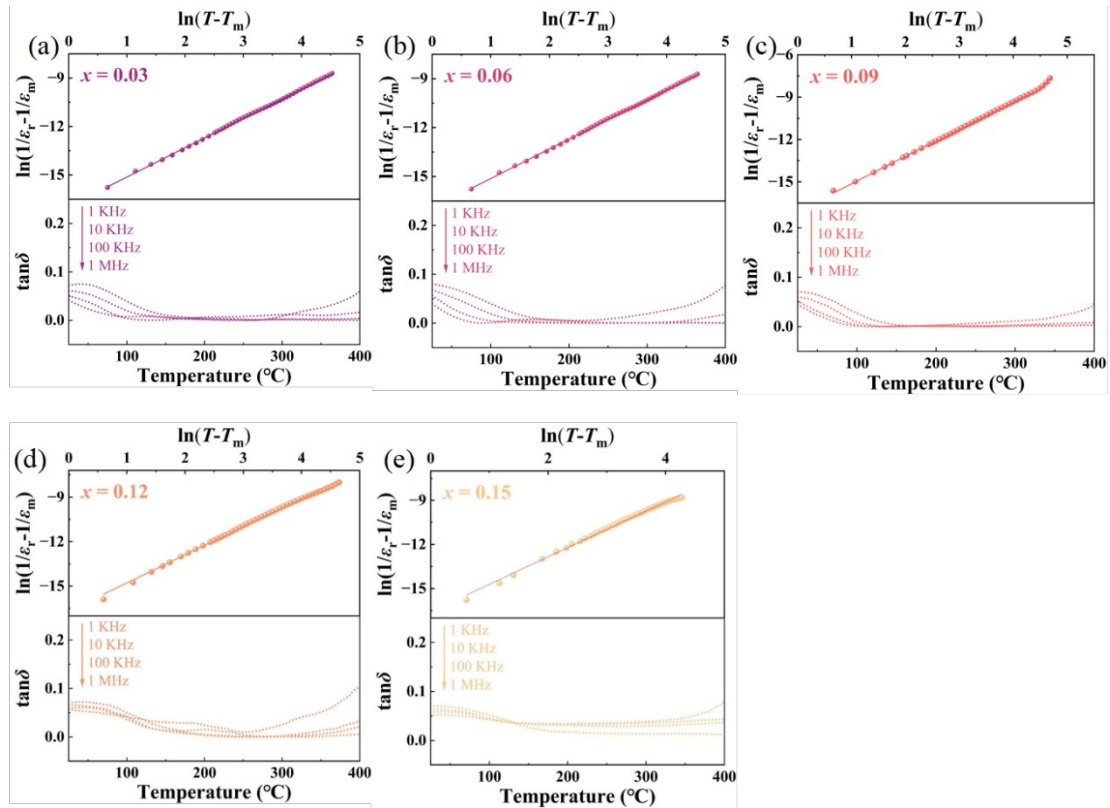


Figure S6. Temperature dependence of the $\tan\delta$ and diffuseness parameter γ for BNLTW- x ceramics, (a) $x = 0.03$, (b) $x = 0.06$, (c) $x = 0.09$, (d) $x = 0.12$, (e) $x = 0.15$.

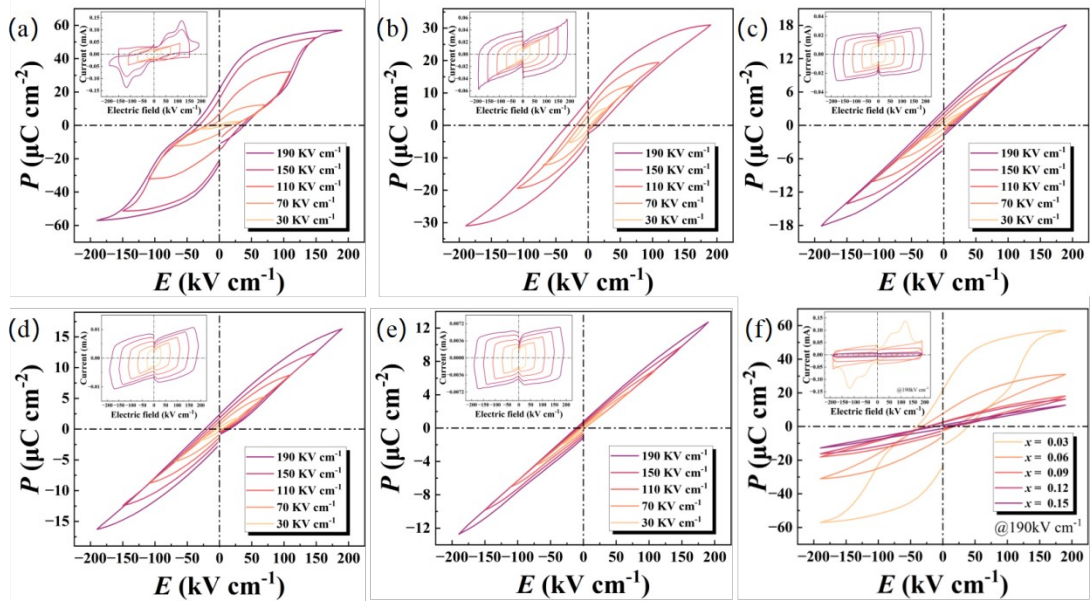


Figure S7. Bipolar P - E hysteresis loops and corresponding I - E loops of BNLTW- x ceramics: (a) $x = 0.03$, (b) $x = 0.06$, (c) $x = 0.09$, (d) $x = 0.12$, (e) $x = 0.15$. (f) Bipolar P - E hysteresis loops and corresponding I - E loops of BNLTW- x ceramics at 190 kV cm $^{-1}$.

Fig. S7(a-e) shows the evolution of P - E hysteresis loops and corresponding I - E curves for BNLTW- x ceramics. It can be seen that at low electric fields, ceramics with low x -content exhibit strong ferroelectricity, while ceramics with high x -content exhibit linear-like properties. As shown in Fig. S7(f), the ceramic ($x = 0.03$) exhibits a wide P - E circle with a large critical electric field E_a [electric field axial intercept, also referred to here as the coercive field (E_c)] of about 37.9 kV cm $^{-1}$, a high residual polarization (P_r) of about 21.5 $\mu\text{C cm}^{-2}$, and a large maximum polarization (P_{\max}) of about 57 $\mu\text{C cm}^{-2}$ when the measured electric field is 190 kV cm $^{-1}$. This result suggests that this composition shows the typical ferroelectric state. Meanwhile, there are four distinct current peaks on the I - E curves, indicating the coexisted nonergodicity and ergodicity. With the introduction of LWT, the pinched P - E loops become slimmer, with the decreased P_{\max} and nearly vanished P_r and E_a . No obvious current peak was detected when $x = 0.09$, 0.12, and 0.15. The deteriorated ferroelectric polarization should be attributed to the increase of the ergodic relaxation state. The polar nanoregions of the ergodic relaxation phase require a higher driving electric field to transform into ferroelectric phase^{1,2}. The results confirm the enhanced ergodicity and suppressed ferroelectricity with the addition of LWT.

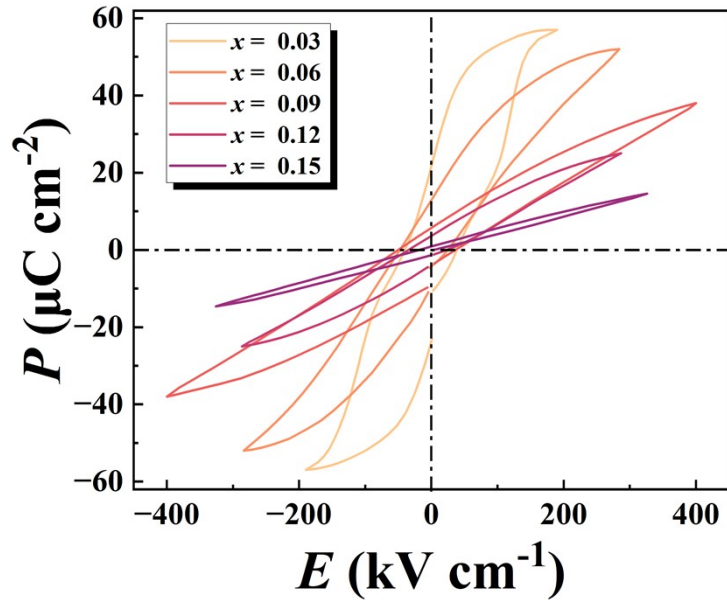


Figure S8. Bipolar P - E hysteresis loops of BNLTW- x ceramics under critical electric field.

Fig. S8 shows the P - E loops of BNLTW- x ($x = 0.03, 0.06, 0.09, 0.12, 0.15$) ceramics measured under the electric field before breakdown. Similar to the unipolar P - E loops, bipolar loops change from fat to thin, and P_r clearly decreases. This may be related to stronger relaxation properties and disruption of long-range order by LWT doping. With the introduction of LWT, the ferroelectric macro-domain vanishes, being replaced with the discrete distribution of PNRs. As the P - E loops become thinner, the E_b greatly improves, increasing from 190 kV cm^{-1} ($x = 0.03$) to 400 kV cm^{-1} ($x = 0.09$).

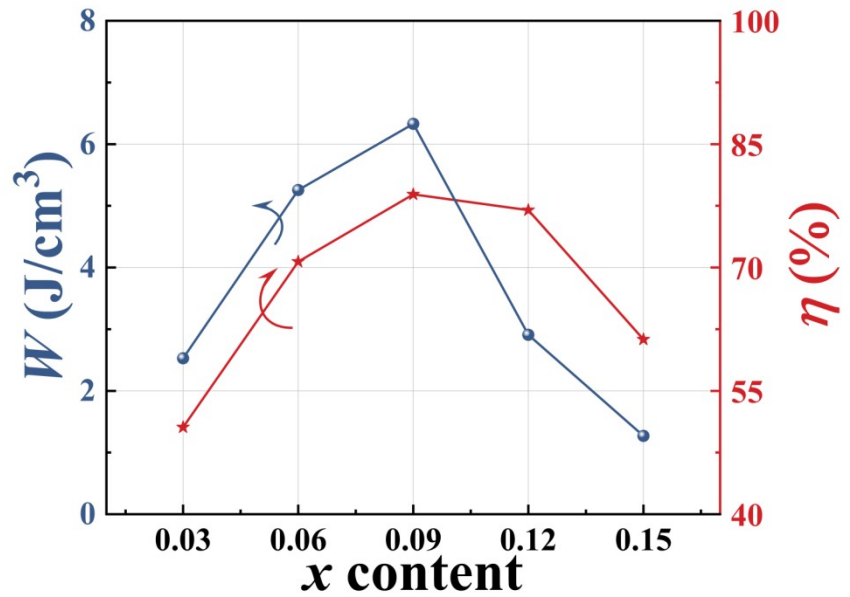


Figure S9. Evolution of recoverable energy storage density and energy efficiency as a function of x .

Table S1. Comparison of the E_b , W_{rec} and η with previous reports.

Composition	E_b (kV cm ⁻¹)	W_{rec} (J cm ⁻³)	η (%)	Ref.
0.7(Na _{0.5} Bi _{0.5}) _{0.7} Sr _{0.3} TiO ₃ -0.3Sr(Ti _{0.85} Zr _{0.15})O ₃	262	3.13	91.14	3
0.85Bi _{0.5} Na _{0.5} TiO ₃ -0.15Ag _{0.91} Sm _{0.03} NbO ₃	170	2.1	83	4
Bi _{0.44} La _{0.06} (Na _{0.82} K _{0.18}) _{0.5} Ti _{0.90-} (Al _{0.5} Nb _{0.5}) _{0.08} Zr _{0.02} O ₃	200	3.24	82	5
[(Bi _{0.5} Na _{0.5}) _{0.93} Ba _{0.07}] _{0.96} La _{0.04} Ti _{0.99} Zr _{0.01} O ₃	100	1.21	74	6
(Na _{0.25} Bi _{0.25} Sr _{0.5})(Ti _{0.8} Sn _{0.2})O ₃	310	3.4	89.5	7
(Bi _{0.5} Na _{0.5}) _{0.94} Ba _{0.06}] _{0.82} La _{0.12} TiO ₃	440	5.93	77.6	8
(Na _{0.5} Bi _{0.5}) _{0.8} Ba _{0.2} Ti _{0.8} Sn _{0.2} O ₃	195	2.35	71.04	9
[Ca _{0.1} (Bi _{0.5} Na _{0.5}) _{0.9}](Ti _{0.85} Zr _{0.15})O ₃	210	2.79	76	10
0.95(0.6Bi _{0.5} Na _{0.5} TiO ₃ -0.4Sr _{0.7} Bi _{0.2} TiO ₃) -0.05AgNbO ₃	246	3.62	89	11
0.9Ba _{0.65} Sr _{0.35} TiO ₃ -0.1Bi(Mg _{2/3} Nb _{1/3})O ₃	400	3.9	85.71	12
0.875BaTiO ₃ -0.125Bi(Mg _{2/3} Nb _{1/3})O ₃	240	1.89	83	13
0.88BaTiO ₃ -0.12Bi(Li _{0.5} Nb _{0.5})O ₃	270	2.032	88	14
BaTiO ₃ -0.06Bi _{2/3} (Mg _{1/3} Nb _{2/3})O ₃	520	4.55	90	15
0.61BiFeO ₃ -0.33(Ba _{0.8} Sr _{0.2})TiO ₃ -0.06La(Mg _{2/3} Nb _{1/3})O ₃	230	3.38	59	16
0.25Bi _{0.83} Sm _{0.17} Fe _{0.95} Sc _{0.05} O _{2.25}	206	3.2	92	17
0.3BiFeO ₃ -0.7(0.88BaTiO ₃ -0.12Bi(Li _{1/3} Hf _{2/3})O ₃)	520	6	90	18
0.9K _{0.5} Na _{0.5} NbO ₃ -0.1BiFeO ₃	206	2	63	19
0.85K _{0.5} Na _{0.5} NbO ₃ -0.15Bi(Zn _{0.5} Zr _{0.5})O ₃	326	3.5	86.8	20
0.8(K _{0.5} Na _{0.5})NbO ₃ -0.2Sr(Sc _{0.5} Nb _{0.5})O ₃	295	2.02	81.4	21
0.9(K _{0.5} Na _{0.5})NbO ₃ -0.1Bi(Mg _{2/3} Nb _{1/3})O ₃	300	4.08	62.7	22

$\text{Ag}_{0.96}\text{Ba}_{0.02}\text{NbO}_3$	350	2.3	46	23
$\text{Ag}_{0.9}\text{Sr}_{0.05}\text{NbO}_3$	190	2.9	56	24
$(\text{Sm}_{0.02}\text{Ag}_{0.94})(\text{Nb}_{0.9}\text{Ta}_{0.1})\text{O}_3$	280	4.87	63.5	25
$\text{Ag}_{0.94}\text{Sm}_{0.02}\text{NbO}_3$	300	4.5	63	26
$0.93\text{NaNbO}_3\text{-}0.07\text{Bi}(\text{Mg}_{0.5}\text{Zr}_{0.5})\text{O}_3$	255	2.31	80.2	27
$\text{Na}_{0.7}\text{Bi}_{0.1}\text{NbO}_3$	203	4.03	85.4	28
$\text{Bi}(\text{Ni}_{0.5}\text{Nb}_{0.5})\text{O}_3$	440	3.31	80.9	29
$\text{NaNbO}_3\text{-}x\text{Bi}(\text{Zn}_{0.5}\text{Zr}_{0.5})\text{O}_3$	371	3.14	84.5	30
BNLTW-0.09	400	6.3	78.9	This work

References

1. A. Deng, J. Wu, *J. Eur. Ceram. Soc.*, 2021, **41**, 5147e54.
2. Y. Ehara, N. Novak, A. Ayrikyan, P.T. Geiger, K.G. Webber. *J. Appl. Phys.*, 2016, **120**, 174103.
3. D. Li, Y. Lin, M. Zhang and H. Yang, *Chem. Eng. J.*, 2020, **392**, 123729.
4. K. Han, N. Luo, Z. Chen, L. Ma, X. Chen, Q. Feng, C. Hu, H. Zhou, Y. Wei and F. Toyohisa, *J. Eur. Ceram. Soc.*, 2020, **40**, 3562-3568.
5. J. Zhang, Y. Lin, L. Wang, Y. Yang, H. Yang and Q. Yuan, *J. Eur. Ceram. Soc.*, 2020, **40**, 5458-5465.
6. X. Lu, J. Xu, L. Yang, C. Zhou, Y. Zhao, C. Yuan, Q. Li, G. Chen and H. Wang, *J. Materomics*, 2016, **2**, 87-93.
7. L. Yang, X. Kong, Z. Cheng and S. Zhang, *J. Mater. Chem. A*, 2019, **7**, 8573-8580.
8. B. Chu, J. Hao, P. Li, Y. Li, W. Li, L. Zheng and H. Zeng, *ACS Appl. Mater. Interfaces*, 2022, **14**, 19683-19696.
9. Y. Pu, L. Zhang, Y. Cui and M. Chen, *ACS Sustain. Chem. Eng.*, 2018, **6**, 6102-6109.
10. Y. Huang, L. Zhang, R. Jing, Q. Hu, D. O. Alikin, V. Y. Shur, S. S. Islam, H. Du, X. Wei, G. Feng, L. Zhang and L. Jin, *Ceram. Int.*, 2021, **47**, 6298-6309.
11. X. Qiao, D. Wu, F. Zhang, B. Chen, X. Ren, P. Liang, H. Du, X. Chao and Z. Yang, *J. Mater. Chem. C*, 2019, **7**, 10514-10520.
12. Z. Dai, J. Xie, W. Liu, X. Wang, L. Zhang, Z. Zhou, J. Li and X. Ren, *ACS Appl. Mater. Interfaces*, 2020, **12**, 30289-30296.
13. G. Liu, Y. Li, M. Shi, L. Yu, P. Chen, K. Yu, Y. Yan, L. Jin, D. Wang and J. Gao, *Ceram. Int.*, 2019, **45**, 19189-19196.
14. W.-B. Li, D. Zhou, L.-X. Pang, R. Xu and H.-H. Guo, *J. Mater. Chem. A*, 2017, **5**, 19607-19612.
15. H. Yang, Z. Lu, L. Li, W. Bao, H. Ji, J. Li, A. Feteira, F. Xu, Y. Zhang, H. Sun, Z. Huang, W. Lou, K. Song, S. Sun, G. Wang, D. Wang and I. M. Reaney, *ACS Appl. Mater. Interfaces*, 2020, **12**, 43942-43949.
16. H. Yang, H. Qi and R. Zuo, *J. Eur. Ceram. Soc.*, 2019, **39**, 2673-2679.
17. Q. Li, S. Ji, D. Wang, J. Zhu, L. Li, W. Wang, M. Zeng, Z. Hou, X. Gao, X. Lu, Q. Li and J.-M. Liu, *J. Eur. Ceram. Soc.*, 2021, **41**, 387-393.
18. J. Zhao, Z. Pan, L. Tang, Y. Shen, X. Chen, H. Li, P. Li, Y. Zhang, J. Liu and J.

- Zhai, *Mater. Today Phys.*, 2022, **27**, 100821.
19. Z. Yang, F. Gao, H. Du, L. Jin, L. Yan, Q. Hu, Y. Yu, S. Qu, X. Wei, Z. Xu and Y.-J. Wang, *Nano Energy*, 2019, **58**, 768-777.
20. M. Zhang, H. Yang, D. Li, L. Ma and Y. Lin, *J. Mater. Chem. C*, 2020, **8**, 8777-8785.
21. L. Zhao, Q. Liu, S. Zhang and J.-F. Li, *J. Mater. Chem. C*, 2016, **4**, 8380-8384.
22. T. Shao, H. Du, H. Ma, S. Qu, J. Wang, J. Wang, X. Wei and Z. Xu, *J. Mater. Chem. A*, 2017, **5**, 554-563.
23. K. Han, N. Luo, Y. Jing, X. Wang, B. Peng, L. Liu, C. Hu, H. Zhou, Y. Wei, X. Chen and Q. Feng, *Ceram. Int.*, 2019, **45**, 5559-5565.
24. K. Han, N. Luo, S. Mao, F. Zhuo, X. Chen, L. Liu, C. Hu, H. Zhou, X. Wang and Y. Wei, *J. Materomics*, 2019, **5**, 597-605.
25. K. Han, N. Luo, S. Mao, F. Zhuo, L. Liu, B. Peng, X. Chen, C. Hu, H. Zhou and Y. Wei, *J. Mater. Chem. A*, 2019, **7**, 26293-26301.
26. J. Gao, Q. Liu, J. Dong, X. Wang, S. Zhang and J.-F. Li, *ACS Appl. Mater. Interfaces*, 2020, **12**, 6097-6104.
27. N. Qu, H. Du, X. Hao. *J. Mater. Chem. C*, 2019, **7**, 7993-8002.
28. M. Zhou, R. Liang, Z. Zhou and X. Dong, *J. Mater. Chem. C*, 2018, **6**, 8528-8537.
29. X. Dong, X. Li, X. Chen, H. Chen, C. Sun, J. Shi, F. Pang and H. Zhou, *Ceram. Int.*, 2021, **47**, 3079-3088.
30. J. Shi, X. Chen, C. Sun, F. Pang, H. Chen, X. Dong, X. Zhou, K. Wang and H. Zhou, *Ceram. Int.*, 2020, **46**, 25731-25737.